AGU PUBLICATIONS

JGR

Journal of Geophysical Research: Solid Earth

RESEARCH ARTICLE
10.1002/2016JB013221

Key Points:
- The b-values of oceanic intraplate earthquakes universally show clear age dependency
- The age dependency is caused by strain rate dependency of b-values at extremely low strain rates

Supporting Information:
- Supporting Information S1
- Data Set S1

Correspondence to:
R. Sasajima,
sasajima@seis.nagoya-u.ac.jp

Citation:
Sasajima, R., and T. Ito (2016), Strain rate dependency of oceanic intraplate earthquake *b*-values at extremely low strain rates, *J. Geophys. Res. Solid Earth*, *121*, 4523–4537, doi:10.1002/2016JB013221.

Received 30 MAY 2016
Accepted 3 JUN 2016
Accepted article online 10 JUN 2016
Published online 29 JUN 2016

Strain rate dependency of oceanic intraplate earthquake *b*-values at extremely low strain rates

Ryohei Sasajima[1] and Takeo Ito[1]

[1] Graduate School of Environmental Studies, Nagoya University, Nagoya, Japan

Abstract We discovered a clear positive dependence of oceanic intraplate earthquake (OCEQ) *b*-values on the age of the oceanic lithosphere. OCEQ *b*-values in the youngest (<10 Ma) oceanic lithosphere are around 1.0, while those in middle to old (>20 Ma) oceanic lithosphere exceed 1.5, which is significantly higher than the average worldwide earthquake *b*-value (around 1.0). On the other hand, the *b*-value of intraplate earthquakes in the Ninety East-Sumatra orogen, where oceanic lithosphere has an anomalously higher strain rate compared with normal oceanic lithosphere, is 0.93, which is significantly lower than the OCEQ *b*-value (about 1.9) with the same age (50–110 Ma). Thus, the variation in *b*-values relates to the strain rate of the oceanic lithosphere and is not caused by a difference in thermal structure. We revealed a negative strain rate dependency of the *b*-value at extremely low strain rates ($< 2 \times 10^{-10}$/year), which can clearly explain the above *b*-values. We propose that the OCEQ *b*-value depends strongly on strain rate (either directly or indirectly) at extremely low strain rates. The high OCEQ *b*-values (> 1.5) in oceanic lithosphere >20 Ma old imply that future improvement in seismic observation will capture many smaller magnitude OCEQs, which will provide valuable information on the evolution of the oceanic lithosphere and the driving mechanism of plate tectonics.

1. Introduction

Oceanic intraplate earthquakes (OCEQs) are intraplate earthquakes that occur in oceanic lithosphere (except outer rise and hot spots) [*Bergman and Solomon*, 1980; *Okal and Sweet*, 2007]. OCEQs provide valuable information regarding the stress state in oceanic lithosphere. Therefore, many studies on OCEQ have attempted to reveal the driving mechanism of plate tectonics from the stress state in the oceanic lithosphere, especially in the 1970s and 1980s [*Sykes and Sbar*, 1973; *Bergman and Solomon*, 1980; *Wiens and Stein*, 1984].

Previous studies suggested that thermal stress caused by the cooling of the oceanic lithosphere and ridge-push forces are especially important sources of differential stress in oceanic lithosphere, i.e., causes of OCEQs [*Turcotte and Oxburgh*, 1973; *Wiens and Stein*, 1984; *Bratt et al.*, 1985; *Bergman*, 1986; *Parmentier and Haxby*, 1986]. The activity of OCEQs is extremely low and decreases with the age of the oceanic lithosphere [*Wiens and Stein*, 1983; *Bergman*, 1986]. The age-dependent generation rate of thermal stress, which reflects the cooling rate of the oceanic lithosphere, may cause this age-dependent seismicity [*Bergman*, 1986; *Kreemer and Gordon*, 2014].

Despite the above mentioned unique features of OCEQs, few recent reports have investigated OCEQ. However, OCEQs are suitable for the statistical analyses of earthquakes with extremely long recurrence intervals because the large surface area of oceanic lithosphere, which covers more than half of the Earth's surface, makes up for the short observation period compared to the recurrence interval of OCEQs.

Accordingly, this paper focuses on the *b*-values of OCEQs. The *b*-value is the slope of the size-frequency relationship of earthquakes, which is known as the Gutenberg-Richter law (GR law) [*Gutenberg and Richter*, 1944]. The GR law is given by $\log_{10} N = a - bM$, where N is the cumulative number of earthquakes with magnitude greater than a magnitude (M) and a and b are constants. Typically, *b*-values are estimated in middle to high seismicity regions because a sufficient number of earthquakes is needed to ensure statistical significance. Thus, the *b*-values of OCEQs provide valuable information related to earthquakes with extremely long recurrence intervals.

Okal and Sweet [2007] reported that the *b*-values of OCEQs do not differ significantly from those of interplate earthquakes. Herein, focusing on age-dependent seismicity in OCEQs, we investigate the *b*-values of OCEQs

based on the age of the oceanic lithosphere. The results show that OCEQ *b*-values have clear age dependency, and we discuss the cause of this finding.

2. Data and Method

2.1. Data Set of OCEQs

We used the EHB bulletin earthquake catalogue from the International Seismological Centre (ISC), in which the hypocenter determinations were improved by the algorithm of *Engdahl et al.* [1998]. The EHB catalogue covers the time period from 1 January 1960 to 31 December 2008. However, to maximize the number of OCEQs with magnitudes greater than the completeness magnitude (M_c), we focused on the time period from 1 January 1966 to 31 December 2008 (discussed in section 3.1). To estimate OCEQ *b*-values, we selected earthquakes that clearly fit the following definition from the EHB catalogue: "an OCEQ occurs in the oceanic region that excludes oceanic ridges, transform faults, outer rises, hot spots, passive margin, and plate-deforming orogens."

We excluded earthquakes that occurred within 120 km of an oceanic ridge and transform plate boundary to exclude earthquakes at oceanic ridges and transform faults. We obtained finely discretized plate boundary digital data by subdividing each of the digital data sets provided by *Bird* [2003] into 100 sections by linear interpolation; we then excluded all earthquakes within 120 km of any subdivided plate boundary data point (this is a modified version of the *Okal and Sweet* [2007] method). This threshold (120 km) is sufficiently larger than the standard deviation of the epicenter location near the ridge listed by the EHB catalogue (maximum = 62.4 km, mean = 20.0 km). For pre-1995 earthquakes near the Eltanin and Udintsev transform faults in the South Pacific Ocean, we used the updated locations of *Okal and Langenhorst* [2000] before 1995 because the EHB catalogue precision is insufficient in that area [*Okal and Langenhorst*, 2000]. We ensured that all selected OCEQs around this region after 1996 were true intraplate earthquakes according to the Global Centroid Moment Tensor (GCMT) solution. We excluded earthquakes within approximately 400 km of the trench axis to exclude outer-rise earthquakes following *Bird* [2003]. This threshold is greater than the observed outer-rise topography and gravity anomaly [*Levitt and Sandwell*, 1995].

We verified the focal mechanism of selected OCEQs that are also listed in the GCMT catalogue to evaluate the possibility of data contamination in the selected OCEQ data set. We confirmed that the probabilities of data interference from ridge earthquakes, transform faulting, and outer-rise earthquakes were extremely low (see Figure S1 in the supporting information).

Next, we excluded earthquakes on hot spots with wide (>100 km) bathymetric anomalies. These were chosen according to present-day hot spots [*Steinberger*, 2000], and the width of the excluded regions corresponded to the width of the bathymetric anomaly. To exclude earthquakes related to plate boundary orogen, we excluded the west central Atlantic orogen, which constitutes the boundary between the North America plate and South America plate [*Bird*, 2003]. We also excluded the Ninety East-Sumatra orogen, which constitutes the boundary between the Indo and Australian plates and a few other plate boundaries under the ocean based on *Bird* [2003] and *Bird et al.* [2015]. We excluded an area near the passive margin identified by a bathymetry anomaly (a few hundreds of kilometers from the coastal line) to exclude any earthquakes related to density anomalies across passive margins. We did not include back-arc basins because compared to normal oceanic lithosphere, they are generated under different conditions related to potential temperature and water content under the spreading axis [e.g., *Wiens et al.*, 2006]. We excluded the 1998 Antarctic earthquake (M_w = 8.1) and its aftershocks, which were possibly caused by stress perturbations associated with deglaciation [*Kreemer and Holt*, 2000]. We also excluded the Gilbert Island swarm, which was an anomalous swarm event, including more than a hundred events (M = 4.6–5.8) between January 1981 and April 1983 [*Lay and Okal*, 1983; *Okal et al.*, 1986]. According to above criteria, we selected 463 OCEQs from the EHB catalogue (Figure 1). A catalogue of the OCEQs selected in this study is provided in Data Set S1 in the supporting information.

2.2. Magnitude Conversion

The EHB earthquake catalogue contains various kinds of magnitude scales, including surface wave magnitude (M_s) and body wave magnitude (m_b). Therefore, we converted these scales to the moment magnitude scale (M_w) as follows.

We used the scalar seismic moment (M_0) directly from the GCMT catalogue for earthquakes that are listed in the GCMT catalogue. For earthquakes with only M_s or m_b listed in the EHB catalogue, M_s and m_b were converted to M_w using exponential regression between the ISC-Global Earthquake Model and the GCMT based on the study of *Di Giacomo et al.* [2015] as $M_w = \exp^{(-0.222+0.233M_s)} + 2.863$ and $M_w = \exp^{(-4.664+0.859m_b)} + 4.555$,

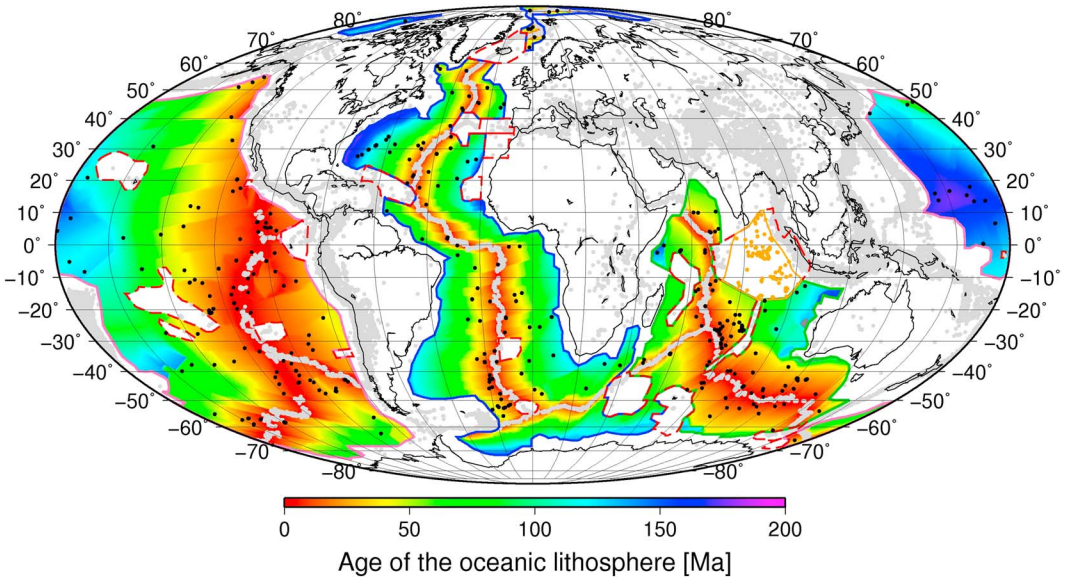

Figure 1. Map of OCEQs containing the age of oceanic lithosphere [*Müller et al.*, 2008]. Black and gray dots indicate the epicenters of OCEQs included herein and other earthquakes from the EHB earthquake catalogue (from 1 January 1966 to 31 December 2008), respectively. Orange dots indicate the epicenters of intraplate earthquakes that occurred in the Ninety East-Sumatra orogen region (for discussion). White regions are outside the OCEQ region. White regions surrounded by red dashed lines indicate hot spot regions, plate boundary orogens, and anomalous event regions. OCEQ regions surrounded by blue, green, and pink lines indicate Indian, Atlantic-Arctic, and Pacific Oceans region, respectively (for Figure 5b).

respectively. For earthquakes with both M_s and m_b listed in the EHB catalogue, we used only M_s for conversion because the regression relationship between m_b and M_w is more scattered than that between M_s and M_w [*Das et al.*, 2011; *Di Giacomo et al.*, 2015]. To convert from M_w to M_0, we used $M_0 = 10^{(1.5M_w+9.1)}$ (Nm) based on the study of *Hanks and Kanamori* [1979].

By evaluating these conversions using OCEQs that are also listed in the GCMT catalogue, we demonstrated that no significant distortion or systematic shift resulted from our conversions (Figure 2).

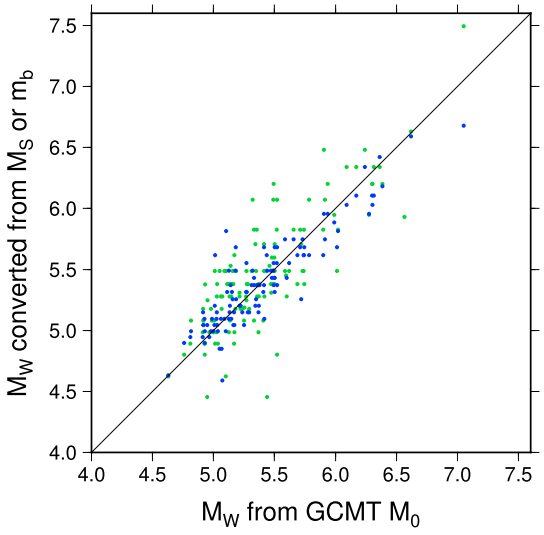

Figure 2. Evaluation of magnitude conversions using earthquakes that are also listed in the GCMT catalogue. The horizontal axis shows the values of M_w determined from M_0 in the GCMT catalogue, and the vertical axis shows M_w values converted from M_s (blue dots) or m_b (green dots) in the EHB catalogue.

2.3. Estimation of *b*-Values

We estimated *b*-values based on the maximum likelihood estimation (MLE) [*Utsu*, 1965; *Aki*, 1965] and determined the standard error using the method of *Shi and Bolt* [1982]. We estimated M_c of the OCEQs using the entire magnitude range (EMR) method [*Woessner and Wiemer*, 2005], modified from *Ogata and Katsura* [1993] (see Appendix A). In the EMR method, M_c is estimated by a grid search as the maximum likelihood of the GR law fitting the entire range of magnitudes (M), considering earthquake detection capability. We chose M_c to be $M_c = 0.1C + 0.05$ (where C is an integer) in both M_s and m_b scales because the M_s and m_b values in the EHB catalogue are reported only to the first decimal place (i.e., the data before conversion had a magnitude range of 0.05). We then evaluated the log likelihood in the EMR method at M_c between 4.05 and 5.95, at intervals of 0.1 for both the M_s

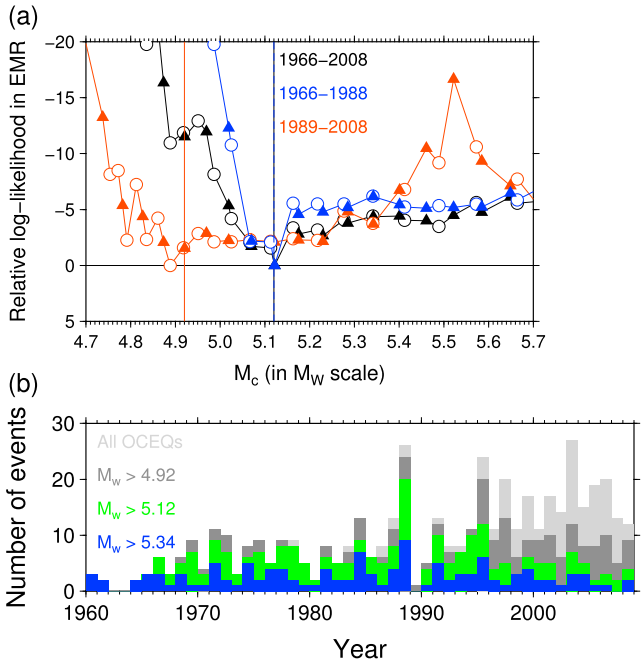

Figure 3. (a) Relative log likelihoods in the EMR method M_c. These are relative values with respect to the maximum log likelihood. We evaluated the log likelihood at M_c between 4.05 and 5.95, at intervals of 0.1 in the M_s scale (solid triangles) and in the m_b scale (open circles), respectively. Black, sky blue, and orange symbols indicate results using the full OCEQ data set (1966–2008), OCEQs in the first half of the time period (1966–1988), and OCEQs in the later half of the time period (1989–2008), respectively. Vertical lines indicate the optimum M_c. (b) Histogram of the annual number of OCEQs with magnitudes greater than 5.34 (blue), 5.12 (green), 4.92 (dark gray), and all OCEQs (light gray).

and m_b scales (Figure 3a). We estimated M_c for three OCEQ date sets. The full data set (1966–2008), the first half of the period (1966–1988), and the later half of the period (1989–2008) are 5.12, 5.12, and 4.92 (in the M_w scale), respectively. To verify the temporal variation of M_c, we plotted the annual number of OCEQs with magnitudes greater than certain levels in Figure 3b. The number of OCEQs with magnitudes greater than 5.12 is stable in time after 1966. Thus, we selected 5.12 (which corresponds to ~4.45 in the M_s scale and ~4.75 in the m_b scale) as the M_c value for estimating OCEQ *b*-values. The total number of OCEQs with magnitudes greater than 5.12 from 1966 to 2008 was 248.

We estimated each *b*-value using 100 earthquakes (with $M > M_c$) ordered from the oldest to the youngest oceanic lithosphere age with 80% overlap (i.e., we shifted the window every 20 earthquakes to a younger age). Using the seafloor age grid data by *Müller et al.* [2008], we investigated the correlation between the age of the oceanic lithosphere and OCEQ *b*-values.

3. Results

The fits of the three OCEQ age windows and all OCEQs with the GR law are provided in Figure 4. Figure 5a shows the *b*-values of OCEQs with respect to the age of the oceanic lithosphere with 80% overlap. These figures show that the OCEQ *b*-values have a clear positive dependency on age. In addition, the OCEQ *b*-values in the middle to older age range (>20 Ma) have anomalously higher values (>1.5) than the universal earthquake *b*-values (~1.0) [e.g., *Kagan*, 1999; *Bird and Kagan*, 2004], and the variation in *b*-values is significantly larger than the standard deviation of each *b*-value.

3.1. Evaluation of the Significance of the Results

To evaluate the significance of these results, we first examined the uncertainty in M_c. Generally, underestimating M_c leads to an underestimation of the *b*-value. Thus, we evaluated the possibility that relatively lower *b*-values around young oceanic lithosphere were artificially caused by the underestimation of M_c. We evaluated how estimated *b*-values vary when M_c is changed (Figures 6 and 7a). Estimated *b*-values of OCEQs in young oceanic lithosphere (0–15 Ma) are stable between 1.05 and 1.2 for a wide range of M_c values between 5.1 and 5.7 (Figure 6). These *b*-values are significantly lower than OCEQ *b*-values for 15–30 Ma and >30 Ma

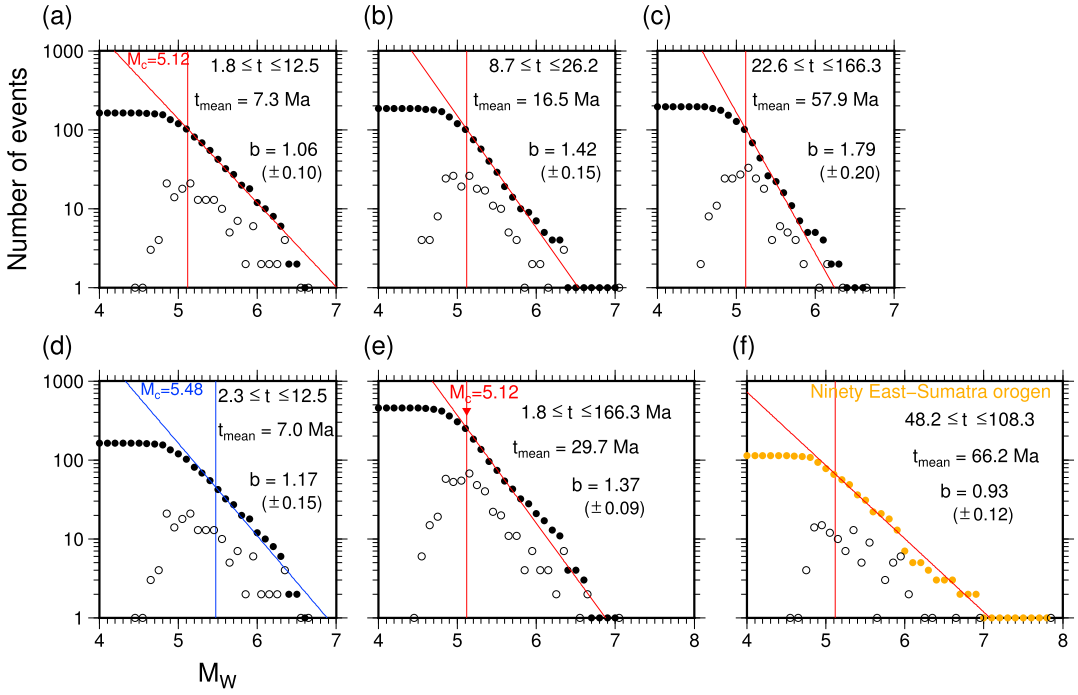

Figure 4. Magnitude-frequency distribution of OCEQs. Solid and white dots indicate the cumulative number of events and noncumulative number of events, respectively. The diagonal line indicates GR law fitting by MLE *b*-value, and the vertical line indicates the assumed M_c. The range of *t* and t_{mean} in each panel indicates the youngest, oldest, and mean age at the hypocenter of OCEQs used for estimating the *b*-value. The *b*-value error is the standard deviation. (a–c) GR law fitting for OCEQs of three different age windows. (d) GR law fitting using the same data set of Figure 4a but assuming M_c = 5.48. (e) GR law fitting for all OCEQs (including 248 earthquakes with magnitudes greater than M_c). (f) GR law fitting for intraplate earthquakes in the Ninety East-Sumatra orogen (Figure 1) for comparison (including 66 earthquakes with magnitudes greater than M_c).

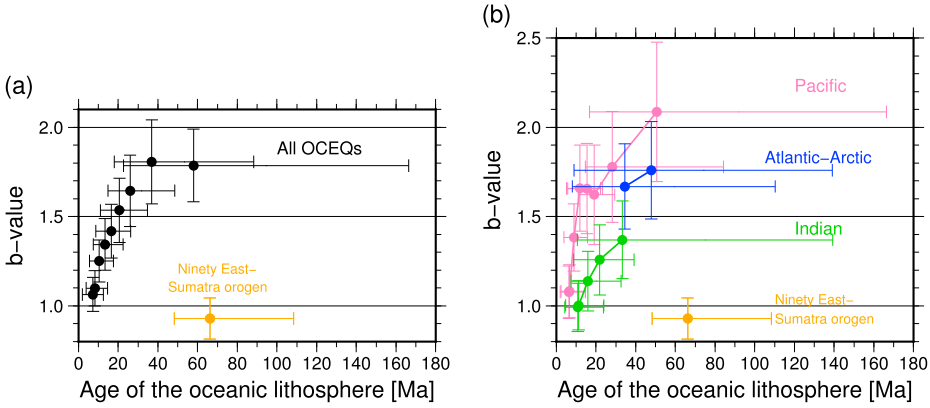

Figure 5. (a) *b*-values with respect to age of the oceanic lithosphere. Black dots indicate OCEQ *b*-values in each age window. The orange dot is the *b*-value of the intraplate earthquake in the Ninety East-Sumatra orogen for comparison. Vertical error bars indicate the standard deviations of the *b*-values. Each dot is plotted at the mean age of OCEQ hypocenters used for estimating the *b*-value, and the horizontal error bars range from the youngest to the oldest age; thus, dots are not always located at the middle of the bar. (b) Same as for Figure 1a, but all OCEQs are divided into three different ocean regions defined in Figure 1. Each age window includes 50 earthquakes and shifts every 10 earthquakes. Note that almost no OCEQs in 0–10 Ma oceanic lithosphere in the Atlantic-Arctic Ocean regions (blue) were selected by our threshold (>120 km from oceanic ridges and transform faults) due to the slow spreading rate of that ridge; therefore, only older OCEQs are resolved.

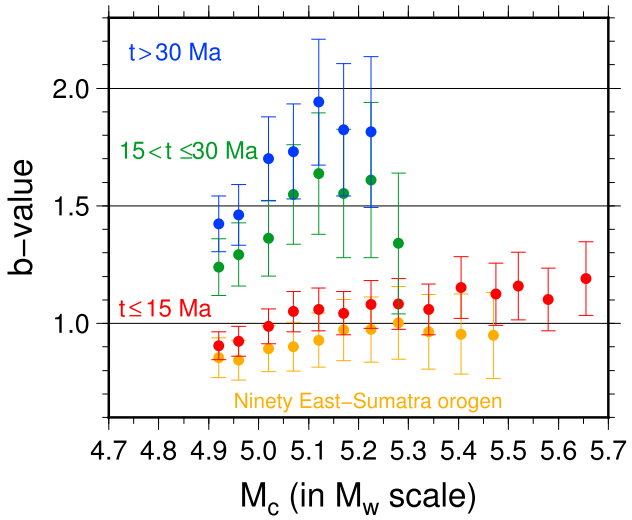

Figure 6. OCEQ *b*-values for different values of M_c, for 0–15 Ma (red), 15–30 Ma (green), >30 Ma (blue), and the Ninety East-Sumatra orogen (orange). Only results where more than 30 earthquakes had magnitudes greater than M_c are shown in order to ensure statistical significance. Therefore, there are no results shown for larger M_c values between 15–30 Ma and >30 Ma.

oceanic lithosphere (1.5–1.6 and 1.5–1.9, respectively). Thus, we confirmed that the age dependence of estimated *b*-values is not due to an underestimation of M_c.

Next, we analyzed the effects of aftershock sequences and swarm-like activities on the estimated *b*-values. We defined swarm and aftershock sequence as earthquakes that satisfy both of next criterions that the distance to the nearest OCEQ hypocenter is less than 100 km, and difference of the occurrence time of each OCEQ is less than 100 days. We found 43 groups containing a total of 140 earthquakes. We defined the main shock in each group as the earthquake with the maximum magnitude, and we did not include the main shock to swarms and aftershocks. The *b*-values obtained with and without the swarms and aftershocks included were similar (Figure 7b).

Next, we estimated *b*-values using individual magnitude scales before conversion (m_b from EHB and M_s from EHB) to evaluate the possibility that OCEQ *b*-value age dependency was a result of magnitude conversion effects. The *b*-values obtained using m_b exhibited a clear age dependency (Figure 7c), as in Figure 5a. The *b*-values obtained using M_s exhibited a similar age dependency, although older ages could not be resolved due to the lack of earthquakes. Thus, OCEQ *b*-value age dependency is not an artifact of magnitude conversion.

These evaluations suggest that the age dependency of OCEQ *b*-values is indeed significant. Further analysis, e.g., on the effect of hypocenter location uncertainty and the age of the oceanic lithosphere on estimated *b*-values, can be found in Appendix B.

3.2. Universality of the Age Dependence Of OCEQ *b*-Values

We divided the ocean region into three regions (Pacific, Indian, and Atlantic-Arctic Oceans) to investigate the universality of the age dependence in OCEQ *b*-values. To increase the age resolution, the width of each

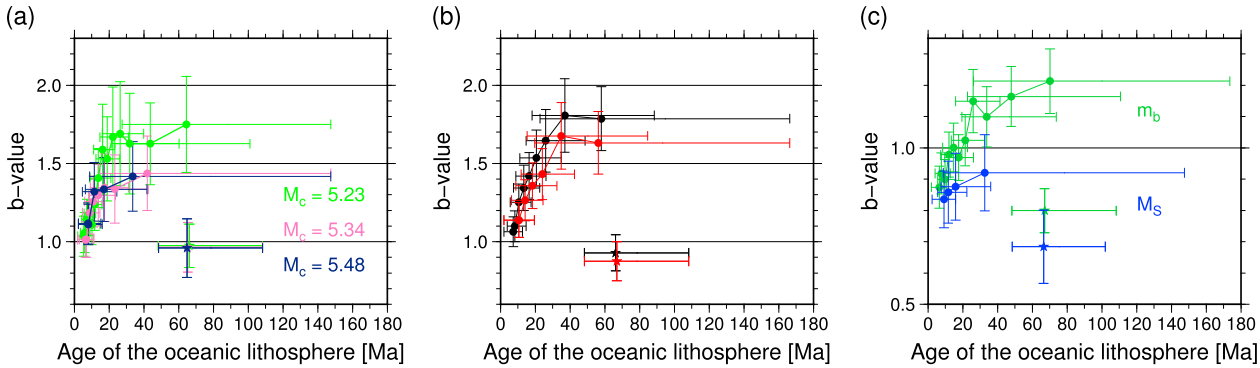

Figure 7. *b*-values of OCEQs (circles) and intraplate earthquakes in the Ninety East-Sumatra orogen (stars), plotted in the same manner as in Figure 5b (each age window includes 50 earthquakes except for the results using m_b in Figure 5c, which each age window includes 100 earthquakes). (a) *b*-values for different values of M_c. (b) *b*-values obtained when swarm and aftershock events were excluded (red symbols). Data from Figure 4a are also included (black symbols). (c) *b*-values estimated using different magnitude scales, i.e., m_b from EHB (green) and M_s from EHB (blue).

window was set at 50 earthquakes. Although the error was large due to the low number of samples, the results were similar for all three regions (Figure 5b), indicating that the age dependency of the OCEQ *b*-values is universal. Compared to the Pacific and Atlantic-Arctic regions, the Indian Ocean region exhibited lower *b*-values; this phenomenon is discussed later.

4. Discussion

4.1. Cause of OCEQ *b*-Value Age Dependency

A clear relationship between *b*-values and the age of the oceanic lithosphere (Figure 5a) indicates the existence of a dominant causal factor. What factor could cause such a strong positive age dependency in *b*-values? Many studies on *b*-values have suggested a negative relationship with differential stress [e.g., *Scholz*, 1968; *Amitrano*, 2003; *Spada et al.*, 2013; *Scholz*, 2015]. However, assuming brittle strength and ductile flow, differential stress in the oceanic lithosphere increases with age because of an accumulation of thermal stress (differential stress in shallower parts is constant because brittle strength is reached at an early age) [e.g., *Wessel*, 1992]. Thus, it is counterproductive to explain increasing *b*-values with age, and we therefore considered other factors.

Thermal structures (such as brittle zone thickness) and strain rate are two possible factors. Brittle zone thickness of the oceanic lithosphere increases with age due to a cooling, and strain rate of the oceanic lithosphere decreases exponentially with age due to a decreasing thermal contraction rate of the oceanic lithosphere [*Kumar and Gordon*, 2009]. To evaluate these two possibilities, we estimated the *b*-values of intraplate earthquakes in the Ninety East-Sumatra orogen (Figure 1). The Ninety East-Sumatra orogen is an old oceanic lithosphere (50–110 Ma) that exhibits anomalously higher strain rates than other oceanic lithosphere of the same age, as inferred from present-day geodetic studies [*Kreemer et al.*, 2014], long-term plate reconstruction [*Gordon et al.*, 1998], and anomalously high seismic activity [e.g., *Wiens et al.*, 1986; *Petroy and Wiens*, 1989; *Stein et al.*, 1990] (discussed in section 4.1.1). These anomalous high strain rates probably arise from high resistance forces due to collision of the Indian plate with the Eurasian plate in the Himalayas [e.g., *Bergman and Solomon*, 1985; *Stein et al.*, 1990]. On the other hand, the thermal structure of this region inferred from the isostatic seafloor depth is similar to that of comparable age oceanic lithosphere [*Crosby and McKenzie*, 2009].

Thus, if the age dependency of OCEQ *b*-values is caused by differences in thermal structure, the *b*-value of intraplate earthquakes in the Ninety East-Sumatra orogen should be large ($b \sim 1.9$ from equivalent age OCEQ *b*-values). Conversely, if the age dependency is caused by differences in strain rate, the *b*-value should be small (e.g., $b \sim 1.0$ from OCEQ *b*-values in the youngest oceanic lithosphere, which has a relatively higher strain rate). Therefore, the *b*-value of intraplate earthquakes in the Ninety East-Sumatra orogen (orange dots in Figure 1; a catalogue of these earthquakes is provided in Data Set S1 in the supporting information) was estimated, not including the Reunion hot spot trace, which has a very high bathymetric anomaly, in order to ensure equivalent structural conditions for comparison. The resulting *b*-value (0.93; Figures 4f and 5a) was significantly lower than the OCEQ *b*-value for the same age (*b*-value ~1.9) and slightly lower than the OCEQ *b*-value in the youngest age window (*b*-value = 1.06). We confirmed that estimated *b*-value is stable between 0.9 and 1.0 even if M_c increased from 5.1 to 5.5, as in Figures 6 and 7a. This result suggests that the age dependency of the *b*-value is not caused by differences in thermal structure. Instead, it may be due to differences in strain rate.

4.1.1. Thermal Elastic Strain Rate in Oceanic Lithosphere

To evaluate the strain rate dependency of OCEQ *b*-values, we estimated the elastic strain rate due to thermal stress at each age of oceanic lithosphere as follows. The important sources of differential stress generation in the oceanic lithosphere (except for orogens) are thermal stress and ridge-push forces [e.g., *Bratt et al.*, 1985; *Wiens and Stein*, 1985]. The rate of stress generation by ridge-push forces (up to 40 MPa at 30 Ma) [*Dahlen*, 1981] is approximately 1 order of magnitude lower than that attributed to thermal stress (up to 300 MPa at 30 Ma) [*Wessel*, 1992]. Thus, for simplicity, we considered only thermal stress as a source of differential stress generation.

To model the thermal evolution of the oceanic lithosphere, we adopted the plate model with parameters from model PS77 [*Parsons and Sclater*, 1977]. We chose model PS77 because the mantle potential temperature in the model (1333°C) is close to estimates from recent studies [*McKenzie et al.*, 2005; *Herzberg et al.*, 2007; *Lee et al.*, 2009]. Following model PS77, we assumed that the thermal conductivity *k* is 3.14 W/m/K and the isothermal depth is 125 km.

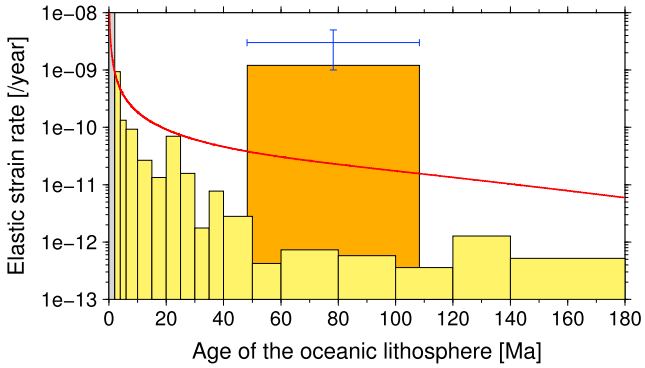

Figure 8. Elastic strain rate against age of the oceanic lithosphere. Red line indicates modeled depth-averaged elastic strain rate in the brittle portion of the oceanic lithosphere caused by thermal stress based on simple modeling. Yellow histogram indicates the elastic strain rate converted from the total seismic moment release rate by observed OCEQs per unit area. We set the width of each bin to include at least 10 OCEQs in order to reduce any perturbation due to the short observation period. Almost no oceanic lithosphere between 0 and 2 Ma old was included in our threshold for OCEQ selection; thus, we could not obtain the corresponding seismic moment release rate (shaded gray). The orange histogram indicates the elastic strain rate from intraplate earthquakes in the Ninety East-Sumatra orogen. The blue bar indicates the range of geodetically estimated strain rates in the Ninety East-Sumatra orogen from the Global Strain Rate Model v2.1 [*Kreemer et al.*, 2014].

The horizontal thermal elastic strain rate ($\dot{E}$) is equivalent to the horizontal strain rate minus the rate of thermal length change, and the horizontal strain rate can be approximated as the depth-averaged rate of thermal length change [*Parmentier and Haxby*, 1986], as follows:

$$\dot{E}(t,z) = \alpha_l \frac{1}{H}\int_0^H \frac{\partial T(t,z)}{\partial t} \mathrm{d}z - \alpha_l \frac{\partial T(t,z)}{\partial t} \tag{1}$$

where t, z, α_l, and T are the age of the oceanic lithosphere, the depth from the seafloor, the linear thermal expansion coefficient (assumed to be $\frac{3.28}{3} \times 10^{-5}$ /K [*Parsons and Sclater*, 1977]), and temperature, respectively. H is the competent lithosphere thickness defined as the thickness at $T < 700$°C [*Parmentier and Haxby*, 1986; *Kumar and Gordon*, 2009]. Most OCEQs occur at $T < 600$°C [*McKenzie et al.*, 2005]; thus, we determined the elastic strain rate for each age of oceanic lithosphere as the depth-averaged elastic strain rate ($\dot{E}_{\mathrm{ave}}$) in brittle zones, as follows:

$$\dot{E}_{\mathrm{ave}}(t) = \frac{1}{D}\int_0^D |\dot{E}(t,z)| \mathrm{d}z \tag{2}$$

where D is the brittle zone thickness at $T < 600$°C. Note that the elastic strain rate considering thermal stress is equivalent to the rate of stress generation divided by the elastic modulus; thus, it differs from the horizontal thermal contraction rate in *Kumar and Gordon* [2009], which corresponds to the strain rate as the first term of the right side of equation (1). The red line in Figure 8 shows the estimated depth-averaged elastic strain rate with respect to the age of the oceanic lithosphere. Estimated $\dot{E}_{\mathrm{ave}}$ decreases with age because the depth-averaged cooling rate of the oceanic lithosphere decreases with age. We also show the range of geodetically estimated strain rates in the Ninety East-Sumatra orogen, which is around $1-5 \times 10^{-9}$/year based on the Global Strain Rate Model (GSRM) v2.1 (second invariant of strain rate) [*Kreemer et al.*, 2014]. Modeled thermal length change rates for the age of the Ninety East-Sumatra orogen (50–110 Ma) are $0-4 \times 10^{-11}$/year, which are negligibly smaller than the strain rates ($1-5 \times 10^{-9}$/year); thus, we can regard the strain rates as equivalent to the elastic strain rates. Therefore, we used the values of $1-5 \times 10^{-9}$/year as the elastic strain rates of the Ninety East-Sumatra orogen. Based on these elastic strain rates, we converted the age in Figure 5a to the elastic strain rate as Figure 9.

In order to evaluate the validity of modeled elastic strain rate, the seismic moment release rate by observed OCEQs per unit area ($\dot{M}_0/A$) is a good index. Based on the formula of *Ward* [1994], which was based on the formula of *Kostrov* [1974], the largest absolute value of the principal components of horizontal strain rate for the brittle portion of the lithosphere is described as follows:

$$|\dot{E}_{\mathrm{max}}| = \frac{\dot{M}_0}{2\mu DA} \tag{3}$$

$\dot{M}_0/A$ is obtained from the total seismic moment release of observed OCEQs divided by the observation period (January 1 1966 to 31 December 2008) and the surface area of the oceanic lithosphere (we show $\dot{M}_0/A$ from

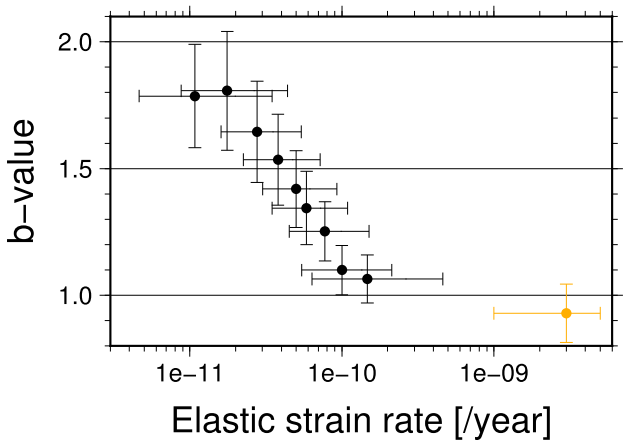

Figure 9. The *b*-values with respect to elastic strain rate (plotted in the same manner as in Figure 5a except that oceanic lithosphere age is replaced with elastic strain rate).

observed OCEQs against age in Figure S2). μ is rigidity, assumed to be 40 GPa, which is the approximate average rigidity of the oceanic crust and the top of the oceanic lithospheric mantle based on the preliminary reference Earth model [*Dziewonski and Anderson*, 1981]. Equation (3) assumes that all elastic strain increments in the brittle portion of the lithosphere are released by observable earthquakes. Thus, $|\dot{E}_{max}|$ in equation (3) does not include the strain released by aseismic fault slip and unobserved, smaller magnitude earthquakes nor long-term elastically stored strain. The $|\dot{E}_{max}|$ values from observed OCEQs in each age window are shown in Figure 8 and decrease exponentially with age. The $|\dot{E}_{max}|$ values are similar to or further smaller than modeled elastic strain rate (about the discrepancy is discussed in the next paragraph). On the other hand, $|\dot{E}_{max}|$ values from intraplate earthquakes in the Ninety East-Sumatra orogen are up to 3 orders of magnitude larger than that of other similar age oceanic lithosphere and are consistent with geodetically estimated strain rates of that area from the GSRM v2.1. Based on these results, we derived the following important points to evaluate *b*-value strain rate dependency: (1) the elastic strain rate in the oceanic lithosphere (except for orogens) decreases exponentially with age; (2) the elastic strain rate in oceanic lithosphere >15 Ma old is extremely low (10^{-12} to 10^{-10}/year); and (3) the elastic strain rate in the Ninety East-Sumatra orogen is significantly larger (2–3 orders of magnitude) than that in equivalent age oceanic lithosphere.

We noted that the elastic strain rate from the observed OCEQs for 10–40 Ma and >40 Ma is 1 and 2 orders of magnitude smaller than our thermal elastic strain rate model, respectively. These discrepancies can be explained by the large *b*-values of OCEQs for >20 Ma. If the *b*-value is around 1.0, the contribution from unobservable, smaller magnitude earthquakes on the total seismic moment release is not significant. However, if the *b*-value exceeds 1.5, the total seismic moment release from smaller magnitude earthquakes is greater than that from larger magnitude earthquakes over the same magnitude range (e.g., seismic moment release by earthquakes with magnitudes between 4.0 and 5.0 is larger than that by earthquakes with magnitudes between 5.0 and 6.0), based on the definition of *b*-value and seismic moment. Thus, the contribution of unobservable, smaller magnitude earthquakes on the total seismic moment release becomes significant for the region where the earthquake *b*-value exceeds 1.5. Therefore, we concluded that most of the seismic moment release in middle to old (>20 Ma) oceanic lithosphere occurs due to unobservable, smaller magnitude OCEQs.

4.1.2. Strain Rate Dependency of OCEQ *b*-Values

Figure 9 shows the relationship between *b*-values and elastic strain rate. The strain rate dependency of the *b*-values can clearly explain both the age dependency of OCEQ *b*-values and the *b*-value of intraplate earthquakes in high strain rate orogen. Conclusively, the age dependency of OCEQ *b*-values is caused by the negative dependence of *b*-value on strain rate at extremely low strain rates. Based on this hypothesis, the relatively low *b*-values in the Indian Ocean's region (Figure 5b) may reflect a relatively high strain rate compared to that of the normal oceanic lithosphere, even outside the estimated diffuse boundary orogen region.

The results also suggest that this strain rate dependency may be weak or perhaps absent at moderate to fast strain rates because the *b*-values for the youngest oceanic lithosphere (strain rate 0.6–4 $\times 10^{-10}$/year, *b*-value = 1.06) and high strain rate orogen (strain rate 1–5 $\times 10^{-9}$/year, *b*-value = 0.93) are not so different, and these are similar to the universal *b*-values (*b*-value ~1.0). Therefore, we supposed that the anomalously high *b*-values are related to the anomalously low strain rates.

4.2. Cause of OCEQ *b*-Value Strain Rate Dependency

How do differences in strain rate cause differences in *b*-values? One clue comes from the observation that a strong strain rate dependency is observed for extremely low strain rates (10^{-10} to 10^{-11}/year). We propose two hypotheses.

The first hypothesis is that differential stress in brittle parts of the oceanic lithosphere decreases as strain rate decreases; consequently, the *b*-values are dependent upon strain rate through the dependence of *b*-value on differential stress. Differential stress is positively related to strain rate if a ductile flow-like stress relaxation mechanism operates in the brittle parts of the oceanic lithosphere. A candidate for such a mechanism is dissolution-precipitation creep, a water-induced chemical deformation that can occur at low temperatures (150–300°C) [e.g., *Shimizu*, 1995; *Wassmann and Stöckhert*, 2013]. If flow viscosity is on the order of 10^{25}–10^{26} Pa s, differential stress depends on strain rate only at condition that strain rate is smaller than 10^{-10}/year (assuming that brittle strength is on the order of approximately 100 MPa), which explains our result. However, if the entire depth range of brittle part of the oceanic lithosphere has this viscosity, the strength of the old oceanic lithosphere would become extremely weak because of the low strain rate. This is not consistent with the observed elastic thickness (10–20 km) of old oceanic lithosphere from seamount loading [*Kalnins and Watts*, 2009; *Zhong and Watts*, 2013]. Thus, even if dissolution-precipitation creep operates in brittle portions of the oceanic lithosphere, its range might be limited in shallower parts (e.g., the oceanic crust) that are rich in pore water. This explanation requires that OCEQs in old oceanic lithosphere occur mainly in the oceanic crust. However, we cannot examine this hypothesis due to the low depth precision of OCEQs in the catalogue. Moreover, if this hypothesis is true, the differential stress in old portions of oceanic lithosphere would be insignificant compared to brittle strength. If this is the case, why do earthquakes occur? Although a special mechanism is required to explain this paradox, *b*-values have been observed to rapidly increase with depth below the brittle ductile transition zone in other regions [*Spada et al.*, 2013]. This observation implies that brittle fractures can also occur in ductile part that differential stress is insignificant compared to brittle strength as a result of unidentified mechanism. The appearance of characteristic features such as waveforms or a stress drop of OCEQs is expected when OCEQs in old oceanic lithosphere occur in extremely low stress regimes. Therefore, this hypothesis can be evaluated through the detailed analysis of OCEQs.

The second hypothesis postulates that extremely low strain rates cause high *b*-values more directly without differential stress dependence. For example, an extremely low stress accumulation rate coincides with a very long earthquake recurrence interval per unit of volume. This provides sufficient time to heal the fault surface via both mechanical and chemical means, even for large faults. If this long-term fault healing changes structures such as the fractal distribution of weak planes in the rock or fractal features of fault surfaces, it may also change the *b*-values. If this occurs, the threshold on the order of 10^{-10}/year must reflect a characteristic time scale of phenomena along the fault surface. We do not have additional suggestions regarding how fault healing creates structures that produce high *b*-values; therefore, this hypothesis is weak. However, if differential stress in brittle portions of old oceanic lithosphere does not decrease much more than in younger portions, another strong connecting factor between *b*-value and strain rate is required; this hypothesis provides such a factor.

4.3. Generality of the Strain Rate Dependency of Earthquake *b*-Values

We questioned whether the strain rate dependency of *b*-values at extremely low strain rates is common to all earthquakes or limited to OCEQs. The strain rate dependency of earthquake *b*-values has not been reported in previous studies in other regions possibly because this phenomenon is only observed in area with extremely low seismicity. Further investigations (e.g., a study on the *b*-values of intraplate earthquakes in stable portions of the continental lithosphere, in which seismicity is extremely low) will provide useful clues to constrain the physical mechanism of the strain rate dependency of OCEQ *b*-values.

4.4. Expectation of Many Smaller Magnitude OCEQs

High *b*-values in >20 Ma oceanic lithosphere imply that there are many unobservable, smaller magnitude OCEQs. Figure 10 shows the magnitude-frequency distribution normalized to the number of events per unit area and time. It is surprising that there are 10 times as many predicted OCEQs with $M > 3.0$ per unit area for 15–30 Ma and >30 Ma than for <15 Ma. We expect that future improvements in M_c or seafloor seismogram observations will capture many smaller magnitude OCEQs in >20 Ma oceanic lithosphere. Since OCEQs contain information regarding the stress state in the oceanic lithosphere [e.g., *Sykes and Sbar*, 1973], the observation of new many smaller magnitude OCEQs will provide valuable information about the evolution of the oceanic lithosphere and enhance our understanding of driving mechanism of plate tectonics.

4.5. Relationship Between Our Results and the Age Dependency of Earthquake *b*-Values in Subduction Zones

Finally, we should note that *Nishikawa and Ide* [2014] suggested that the *b*-values of earthquakes near subduction zones are positively dependent upon age of subducting oceanic lithosphere. This result seems to be

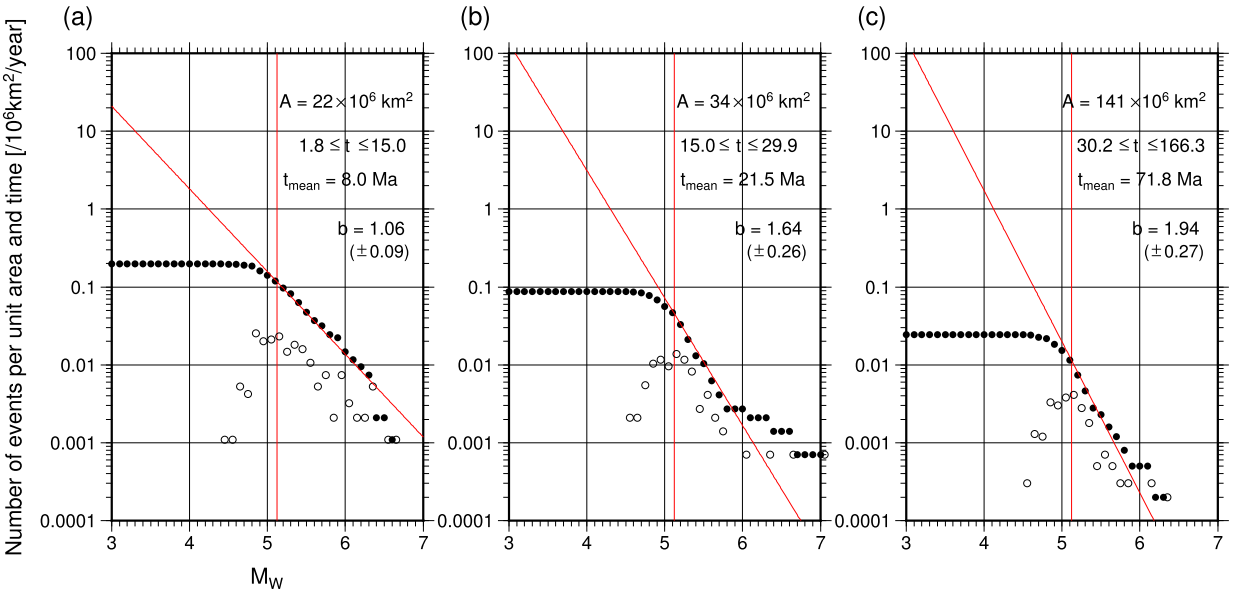

Figure 10. Magnitude-frequency distribution normalized by unit area of the oceanic lithosphere and unit time. "*A*" is the total area of the oceanic lithosphere defined as the OCEQ region in Figure 1, (a) for ≤ 15 Ma, (b) for 15–30 Ma, and (c) for >30 Ma. Other parameters are the same as in Figure 4a.

similar to the findings of this study. However, they attributed the dependency to differences in differential stress around subduction zones caused by differences in slab buoyancy with age. Therefore, their conclusion does not relate to our results. Similarly, our conclusions do not affect their interpretation because our results indicate that *b*-values do not depend on thermal structure but on strain rate.

5. Conclusions

The *b*-values of OCEQs exhibit a clear positive correlation with the age of the oceanic lithosphere. The OCEQ *b*-values in the youngest (<10 Ma) oceanic lithosphere are around 1.0, while those in middle to older age (>20 Ma) oceanic lithosphere exceed 1.5, which is significantly higher than the global earthquake *b*-value (~1.0). These features are found universally in all three major ocean regions. On the other hand, the *b*-value in the Ninety East-Sumatra orogen, where the oceanic lithosphere has an anomalously higher strain rate than normal oceanic lithosphere, is 0.93, which is significantly lower than OCEQ *b*-values (around 1.9) with the same age (50–110 Ma). Therefore, the variation of *b*-values does not result from differences in thermal structure but instead is attributed to differences in strain rate. We revealed that existence of negative strain rate dependency of OCEQ *b*-values in extremely low strain rates ($< 2\times10^{-10}$/year) can clearly explain these *b*-values. We propose that OCEQ *b*-values (and possibly earthquake *b*-values) strongly depend on strain rate at extremely low strain rates, either directly or indirectly.

The high OCEQ *b*-values (> 1.5) in oceanic lithosphere >20 Ma old imply the existence of many unobservable smaller magnitude OCEQs, which will provide valuable information on the evolution of the oceanic lithosphere and the driving mechanism of plate tectonics.

Appendix A: Entire Magnitude Range (EMR) Method

In the EMR method, completeness magnitude (M_c) is estimated as the maximum likelihood of the GR law fitting the entire range of magnitude (M) considering earthquake detection capability [*Woessner and Wiemer*, 2005] as follows. A detection capability $q(M|\mu,\sigma)$ was multiplied by the expected occurrence frequency from the GR law fitting for data ($M < M_c$). Standard MLE *b*-values [*Utsu*, 1965; *Aki*, 1965] were used for the GR law fitting using earthquakes with $M \geq M_c$. $q(M|\mu,\sigma)$ was assumed to be the cumulative normal distribution [*Woessner and Wiemer*, 2005] given by

$$q(M|\mu,\sigma) = \begin{cases} \dfrac{1}{\sigma\sqrt{2\pi}} \displaystyle\int_{-\infty}^{M} \exp\left(-\frac{(x-\mu)^2}{2\sigma^2}\right) \mathrm{d}x & (M < M_c) \\ 1 & (M \geq M_c) \end{cases} \tag{A1}$$

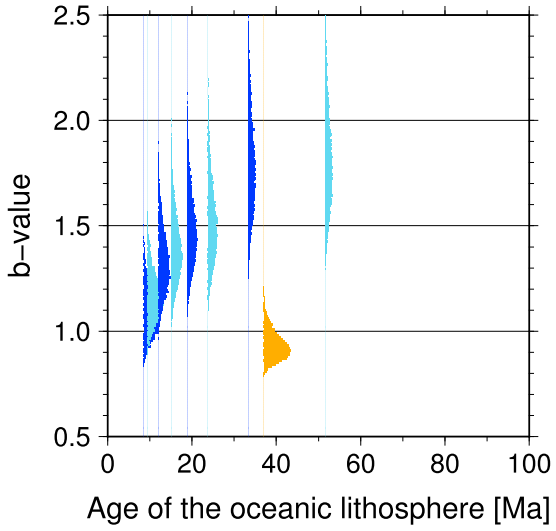

Figure B1. Histogram of estimated *b*-values performed 10,000 times for each age window of OCEQs (blue and sky blue colors are used alternately to avoid overlaps in the plot) and intraplate earthquakes in the Ninety East-Sumatra orogen (orange). Note that age windows and the aspect ratio of the figure differ slightly from Figure 5.

where μ indicates the magnitude at which 50% of earthquakes are detected and σ is the standard deviation to describe the steepness of decreasing detectability of earthquakes. The values of μ and σ along with the *b*-value were estimated by MLE.

Appendix B: Additional Statistical Tests

We performed additional statistical tests to evaluate the uncertainty in estimated *b*-values. First, we numerically estimated the error in estimated *b*-values as follows. We made age windows, with each window including 120 OCEQs with $M > M_c$, and we shifted the window from the oldest age to younger ages every 20 OCEQs. We randomly chose 100 OCEQs from the 120 OCEQs and estimated the *b*-values for each age window. For the Ninety East-Sumatra orogen, we randomly chose 50 earthquakes from all 66 earthquakes and estimated the *b*-values. We performed these estimations 10,000 times and obtained the histogram of estimated *b*-values shown in Figure B1, thereby confirming the significance of our results.

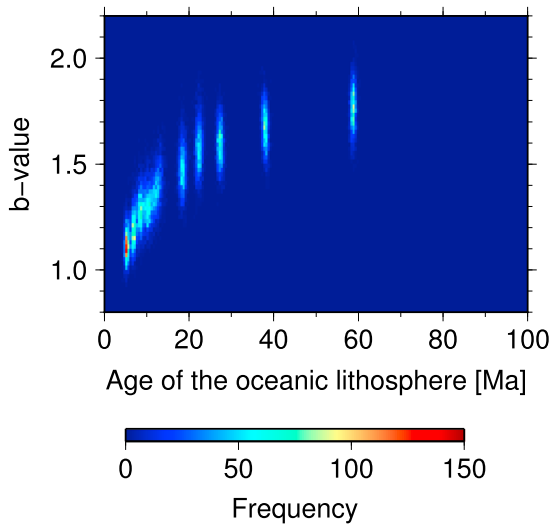

Figure B2. Frequency of estimated *b*-value at mean OCEQ hypocenter age for nine age windows and 10,000 iterations (for details see text in Appendix B). One grid size is 0.5 Ma for age and 0.02 for *b*-values.

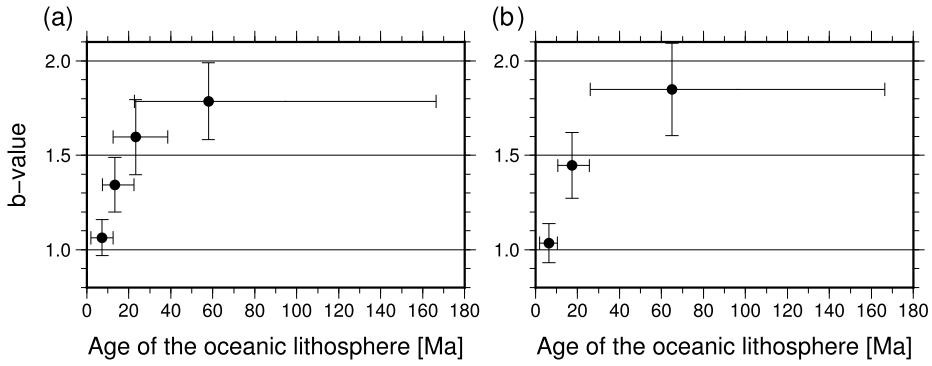

Figure B3. Same as Figure 5a except with a different overlap range of the age windows. (a) Each age window includes 100 earthquakes, as in Figure 5a, but the age window moves every 50 earthquakes from older to younger ages (i.e., 50% overlap). (b) Nonoverlapping age windows. Each age window includes 83 earthquakes (except for the youngest age, which includes 82 earthquakes).

Next, we evaluated the effects of uncertainty in the hypocenter location and age of the oceanic lithosphere on our results. We added normal random numbers to the horizontal hypocenter locations of OCEQs based on horizontal hypocenter location errors for each OCEQ listed in the EHB catalogue and simultaneously added normal random numbers to the age of the oceanic lithosphere based on the age error grid data by *Müller et al.* [2008]. The age error is less than 1 Ma for most areas, but some areas have an error of ~10 Ma. The mean horizontal hypocenter error in the EHB catalogue is ~20 km, which gives an age error of 0.1–0.5 Ma. The most notable variation in this simulation is whether or not an OCEQ was detected by our threshold (>120 km from ridge axis and transform faults). We set each age window to include 100 OCEQs and shifted the age window from the youngest age to older ages for every 20 earthquakes until the fifth age window. Similarly, we made four age windows from the oldest age to younger ages. We estimated *b*-values for these nine age windows. We plotted estimated *b*-values for the mean OCEQ hypocenter age for 10,000 iterations in Figure B2. The nine peaks correspond to the nine age windows. The result indicates that errors in hypocenter location and age do not affect estimated *b*-values.

Figure B3 shows a different overlap range of age windows to Figure 5a. These figures display how the relationship between OCEQ *b*-value and age vary according to different age windows. The nonoverlapped figure indicates that OCEQ *b*-values gradually increase with age (i.e., as strain rate decreases).

Acknowledgments
We used the EHB Bulletin earthquake catalogue of ISC and the GCMT catalog of the GCMT project. All figures were created using the Generic Mapping Tools software by *Wessel and Smith* [1991]. We would like to thank two anonymous reviewers and the Editor M. Savage for their helpful comments.

References

Aki, K. (1965), Maximum likelihood estimate of b in the formula $logN = a - bM$ and its confidence limits, *Bull. Earthquake Res. Inst.*, *43*, 237–239.

Amitrano, D. (2003), Brittle-ductile transition and associated seismicity: Experimental and numerical studies and relationship with the b value, *J. Geophys. Res.*, *108*(B1), 2044, doi:10.1029/2001JB000680.

Bergman, E. A. (1986), Intraplate earthquakes and the state of stress in oceanic lithosphere, *Tectonophysics*, *132*(1), 1–35, doi:10.1016/0040-1951(86)90022-3.

Bergman, E. A., and S. C. Solomon (1980), Oceanic intraplate earthquakes: Implications for local and regional intraplate stress, *J. Geophys. Res.*, *85*(B10), 5389–5410, doi:10.1029/JB085iB10p05389.

Bergman, E. A., and S. C. Solomon (1985), Earthquake source mechanisms from body-waveform inversion and intraplate tectonics in the northern Indian Ocean, *Phys. Earth Planet. Inter.*, *40*(1), 1–23, doi:10.1016/0031-9201(85)90002-0.

Bird, P. (2003), An updated digital model of plate boundaries, *Geochem. Geophys. Geosyst.*, *4*(3), 1027, doi:10.1029/2001GC000252.

Bird, P., and Y. Y. Kagan (2004), Plate-tectonic analysis of shallow seismicity: Apparent boundary width, beta, corner magnitude, coupled lithosphere thickness, and coupling in seven tectonic settings, *Bull. Seismol. Soc. Am.*, *94*(6), 2380–2399, doi:10.1785/0120030107.

Bird, P., D. Jackson, Y. Kagan, C. Kreemer, and R. Stein (2015), GEAR1: A global earthquake activity rate model constructed from geodetic strain rates and smoothed seismicity, *Bull. Seismol. Soc. Am.*, *105*(5), 2538–2554, doi:10.1785/0120150058.

Bratt, S. R., E. A. Bergman, and S. C. Solomon (1985), Thermoelastic stress: How important as a cause of earthquakes in young oceanic lithosphere?, *J. Geophys. Res.*, *90*(B12), 10,249–10,260, doi:10.1029/JB090iB12p10249.

Crosby, A. G., and D. McKenzie (2009), An analysis of young ocean depth, gravity and global residual topography, *Geophys. J. Int.*, *178*(3), 1198–1219, doi:10.1111/j.1365-246X.2009.04224.x.

Dahlen, F. (1981), Isostasy and the ambient state of stress in the oceanic lithosphere, *J. Geophys. Res.*, *86*(B9), 7801–7807, doi:10.1029/JB086iB09p07801.

Das, R., H. Wason, and M. Sharma (2011), Global regression relations for conversion of surface wave and body wave magnitudes to moment magnitude, *Nat. Hazards*, *59*(2), 801–810, doi:10.1007/s11069-011-9796-6.

Di Giacomo, D., I. Bondár, D. A. Storchak, E. R. Engdahl, P. Bormann, and J. Harris (2015), ISC-GEM: Global instrumental earthquake catalogue (1900–2009), III. Re-computed M_s and m_b, proxy M_w, final magnitude composition and completeness assessment, *Phys. Earth Planet. Inter.*, *239*, 33–47, doi:10.1016/j.pepi.2014.06.005.

Dziewonski, A. M., and D. L. Anderson (1981), Preliminary reference Earth model, *Phys. Earth Planet. Inter.*, *25*(4), 297–356, doi:10.1016/0031-9201(81)90046-7.
Engdahl, E. R., R. van der Hilst, and R. Buland (1998), Global teleseismic earthquake relocation with improved travel times and procedures for depth determination, *Bull. Seismol. Soc. Am.*, *88*(3), 722–743.
Gordon, R. G., C. DeMets, and J.-Y. Royer (1998), Evidence for long-term diffuse deformation of the lithosphere of the equatorial Indian Ocean, *Nature*, *395*(6700), 370–374, doi:10.1038/26463.
Gutenberg, B., and C. F. Richter (1944), Frequency of earthquakes in California, *Bull. Seismol. Soc. Am.*, *34*(4), 185–188.
Hanks, T. C., and H. Kanamori (1979), A moment magnitude scale, *J. Geophys. Res.*, *84*(B5), 2348–2350, doi:10.1029/JB084iB05p02348.
Herzberg, C., P. D. Asimow, N. Arndt, Y. Niu, C. Lesher, J. Fitton, M. Cheadle, and A. Saunders (2007), Temperatures in ambient mantle and plumes: Constraints from basalts, picrites, and komatiites, *Geochem. Geophys. Geosyst.*, *8*, Q02006, doi:10.1029/2006GC001390.
Kagan, Y. (1999), Universality of the seismic moment-frequency relation, *Pure Appl. Geophys.*, *155*, 537–573, doi:10.1007/978-3-0348-8677-216.
Kalnins, L., and A. Watts (2009), Spatial variations in effective elastic thickness in the western Pacific ocean and their implications for Mesozoic volcanism, *Earth Planet. Sci. Lett.*, *286*(1), 89–100, doi:10.1016/j.epsl.2009.06.018.
Kostrov, V. V. (1974), Seismic moment and energy of earthquakes and seismic flow of rock [English Transl.], *Izv. Acad. Sci. USSR Phys. Solid Earth*, *1*, 13–21.
Kreemer, C., and R. G. Gordon (2014), Pacific plate deformation from horizontal thermal contraction, *Geology*, *42*(10), 847–850, doi:10.1130/G35874.1.
Kreemer, C., and W. E. Holt (2000), What caused the March 25, 1998 Antarctic plate earthquake?: Inferences from regional stress and strain rate fields, *Geophys. Res. Lett.*, *27*(15), 2297–2300, doi:10.1029/1999GL011188.
Kreemer, C., G. Blewitt, and E. C. Klein (2014), A geodetic plate motion and global strain rate model, *Geochem. Geophys. Geosyst.*, *15*, 3849–3889, doi:10.1002/2014GC005407.
Kumar, R. R., and R. G. Gordon (2009), Horizontal thermal contraction of oceanic lithosphere: The ultimate limit to the rigid plate approximation, *J. Geophys. Res.*, *114*, B01403, doi:10.1029/2007JB005473.
Lay, T., and E. Okal (1983), The Gilbert islands (republic of Kiribati) earthquake swarm of 1981–1983, *Phys. Earth Planet. Inter.*, *33*(4), 284–303, doi:10.1016/0031-9201(83)90046-8.
Lee, C.-T. A., P. Luffi, T. Plank, H. Dalton, and W. P. Leeman (2009), Constraints on the depths and temperatures of basaltic magma generation on Earth and other terrestrial planets using new thermobarometers for mafic magmas, *Earth Planet. Sci. Lett.*, *279*(1), 20–33, doi:10.1016/j.epsl.2008.12.020.
Levitt, D. A., and D. T. Sandwell (1995), Lithospheric bending at subduction zones based on depth soundings and satellite gravity, *J. Geophys. Res.*, *100*(B1), 379–400, doi:10.1029/94JB02468.
McKenzie, D., J. Jackson, and K. Priestley (2005), Thermal structure of oceanic and continental lithosphere, *Earth Planet. Sci. Lett.*, *233*(3), 337–349, doi:10.1016/j.epsl.2005.02.005.
Müller, R. D., M. Sdrolias, C. Gaina, and W. R. Roest (2008), Age, spreading rates, and spreading asymmetry of the world's ocean crust, *Geochem. Geophys. Geosyst.*, *9*, Q04006, doi:10.1029/2007GC001743.
Nishikawa, T., and S. Ide (2014), Earthquake size distribution in subduction zones linked to slab buoyancy, *Nat. Geosci.*, *7*(12), 904–908, doi:10.1038/ngeo2279.
Ogata, Y., and K. Katsura (1993), Analysis of temporal and spatial heterogeneity of magnitude frequency distribution inferred from earthquake catalogues, *Geophys. J. Int.*, *113*(3), 727–738, doi:10.1111/j.1365-246X.1993.tb04663.x.
Okal, E. A., and A. R. Langenhorst (2000), Seismic properties of the Eltanin transform system, south Pacific, *Phys. Earth Planet. Inter.*, *119*(3), 185–208, doi:10.1016/S0031-9201(99)00169-7.
Okal, E. A., and J. R. Sweet (2007), Frequency-size distributions for intraplate earthquakes, *Geol. Soc. Am. Spec. Pap.*, *425*, 59–71, doi:10.1130/2007.2425(05).
Okal, E. A., D. F. Woods, and T. Lay (1986), Intraplate deformation in the Samoa-Gilbert-Ralik area: A prelude to a change of plate boundaries in the southwest Pacific?, *Tectonophysics*, *132*(1), 69–77, doi:10.1016/0040-1951(86)90025-9.
Parmentier, E. M., and W. F. Haxby (1986), Thermal stresses in the oceanic lithosphere: Evidence from geoid anomalies at fracture zones, *J. Geophys. Res.*, *91*(B7), 7193–7204, doi:10.1029/JB091iB07p07193.
Parsons, B., and J. G. Sclater (1977), An analysis of the variation of ocean floor bathymetry and heat flow with age, *J. Geophys. Res.*, *82*(5), 803–827, doi:10.1029/JB082i005p00803.
Petroy, D. E., and D. A. Wiens (1989), Historical seismicity and implications for diffuse plate convergence in the northeast Indian Ocean, *J. Geophys. Res.*, *94*(B9), 12,301–12,319, doi:10.1029/JB094iB09p12301.
Scholz, C. (1968), The frequency-magnitude relation of microfracturing in rock and its relation to earthquakes, *Bull. Seismol. Soc. Am.*, *58*(1), 399–415.
Scholz, C. H. (2015), On the stress dependence of the earthquake b value, *Geophys. Res. Lett.*, *42*(5), 1399–1402, doi:10.1002/2014GL062863.
Shi, Y., and B. A. Bolt (1982), The standard error of the magnitude-frequency b value, *Bull. Seismol. Soc. Am.*, *72*(5), 1677–1687.
Shimizu, I. (1995), Kinetics of pressure solution creep in quartz: Theoretical considerations, *Tectonophysics*, *245*(3), 121–134, doi:10.1016/0040-1951(94)00230-7.
Spada, M., T. Tormann, S. Wiemer, and B. Enescu (2013), Generic dependence of the frequency-size distribution of earthquakes on depth and its relation to the strength profile of the crust, *Geophys. Res. Lett.*, *40*, 709–714, doi:10.1029/2012GL054198.
Stein, C. A., S. Cloetingh, and R. Wortel (1990), Kinematics and mechanics of the Indian ocean diffuse plate boundary zone, *Proc. Ocean Drill Prog. Sci. Results*, *116*, 261–277.
Steinberger, B. (2000), Plumes in a convecting mantle: Models and observations for individual hotspots, *J. Geophys. Res.*, *105*(B5), 11,127–11,152, doi:10.1029/1999JB900398.
Sykes, L. R., and M. L. Sbar (1973), Intraplate earthquakes, lithospheric stresses and the driving mechanism of plate tectonics, *Nature*, *245*, 298–302, doi:10.1038/245298a0.
Turcotte, D. L., and E. R. Oxburgh (1973), Mid-plate tectonics, *Nature*, *244*, 337–339, doi:10.1038/244337a0.
Utsu, T. (1965), A method for determining the value of b in a formula $logN = a - bM$ showing the magnitude-frequency relation for earthquakes [in Chinese], *Geophys. Bull. Hokkaido Univ.*, *13*, 99–103.
Ward, S. N. (1994), A multidisciplinary approach to seismic hazard in southern California, *Bull. Seismol. Soc. Am.*, *84*(5), 1293–1309.
Wassmann, S., and B. Stöckhert (2013), Rheology of the plate interface—Dissolution precipitation creep in high pressure metamorphic rocks, *Tectonophysics*, *608*, 1–29, doi:10.1016/j.tecto.2013.09.030.
Wessel, P. (1992), Thermal stresses and the bimodal distribution of elastic thickness estimates of the oceanic lithosphere, *J. Geophys. Res.*, *97*(B10), 14,177–14,193, doi:10.1029/92JB01224.

Wessel, P., and W. H. F. Smith (1991), Free software helps map and display data, *Eos Trans. AGU*, *72*(41), 441–446, doi:10.1029/90EO00319.
Wiens, D. A., and S. Stein (1983), Age dependence of oceanic intraplate seismicity and implications for lithospheric evolution, *J. Geophys. Res.*, *88*(B8), 6455–6468, doi:10.1029/JB088iB08p06455.
Wiens, D. A., and S. Stein (1984), Intraplate seismicity and stresses in young oceanic lithosphere, *J. Geophys. Res.*, *89*(B13), 11,442–11,464, doi:10.1029/JB089iB13p11442.
Wiens, D. A., and S. Stein (1985), Oceanic lithosphere implications of oceanic intraplate seismicity for plate stresses, driving forces and rheology, *Tectonophysics*, *116*(1), 143–162, doi:10.1016/0040-1951(85)90227-6.
Wiens, D. A., S. Stein, C. Demets, R. G. Gordon, and C. Stein (1986), Plate tectonic models for Indian Ocean "intraplate" deformation, *Tectonophysics*, *132*(1), 37–48, doi:10.1016/0040-1951(86)90023-5.
Wiens, D. A., K. A. Kelley, and T. Plank (2006), Mantle temperature variations beneath back-arc spreading centers inferred from seismology, petrology, and bathymetry, *Earth Planet. Sci. Lett.*, *248*(1), 30–42, doi:10.1016/j.epsl.2006.04.011.
Woessner, J., and S. Wiemer (2005), Assessing the quality of earthquake catalogues: Estimating the magnitude of completeness and its uncertainty, *Bull. Seismol. Soc. Am.*, *95*(2), 684–698, doi:10.1785/0120040007.
Zhong, S., and A. B. Watts (2013), Lithospheric deformation induced by loading of the Hawaiian islands and its implications for mantle rheology, *J. Geophys. Res. Solid Earth*, *118*, 6025–6048, doi:10.1002/2013JB010408.